

# Optical surface plasmons at a metal-crystal interface with the Drude-Lorentz model for material permittivity

A. P. Misra,<sup>1,\*</sup> M. Shahmansouri,<sup>2,†</sup> and N. Khoddam<sup>2,‡</sup>

<sup>1</sup>*Department of Mathematics, Siksha Bhavana, Visva-Bharati (A Central University), Santiniketan-731 235, India*

<sup>2</sup>*Department of Physics, Faculty of Science, Arak University, Arak, P.O. Box 38156-8-8349, Iran*

The theory of surface electromagnetic waves (SEMWs) propagating at optical frequencies along the interface of an isotropic noble metal [e.g., gold (Au)] and a uniaxial crystal [e.g., Rutile (TiO<sub>2</sub>)] is revisited with the Drude-Lorentz (DL) model for the complex dielectric material permittivity ( $\epsilon_p$ ). The latter accounts for the contributions of both the *intraband* transitions of the free electrons and the multiple *interband* transitions of the bound electrons in metals. The propagation characteristics of the wave vectors and wave frequency of SEMWs, the hybridization factors, i.e., the amplitude ratios between the transverse-electric (TE) and transverse-magnetic (TM) modes in the isotropic metal, and between the ordinary and extraordinary modes in the uniaxial substrate are studied numerically. It is found that the results are significantly modified from those with the Drude model for  $\epsilon_p$ , especially in the short-wavelength spectra ( $\lambda \lesssim 500$  nm) and with a small deviation of the orientation of the optical axis. The excitation of such SEMWs can have novel applications in transportation of EM signals in a specified direction at optical frequencies ( $\sim$  PHz).

## I. INTRODUCTION

The interaction between electromagnetic (EM) waves and isotropic metals is ascertained by the collective movements of free electrons (in the long-wavelength spectra  $> 500$  nm) as well as multiple interband transitions of bound electrons (in the short-wavelength spectra  $\lesssim 500$  nm) in metals. The optical and transport properties of the latter are usually described by the complex permittivity function ( $\epsilon_p$ ) of the wave frequency and wave vector. The simple models for  $\epsilon_p$  are, e.g., the Drude model and the Linhard model [1] which account for only the *intraband* transition of free electrons in metals. However, for a practical metal, in addition to this *intraband* transition, there are usually multiple *interband* transitions of the bound electrons that are excited by the high-energy photons. So, in the short-wavelength spectra ( $\lambda < 500$  nm), the dielectric function can no longer be accurately described by the Drude or Linhard models but can be well described by the Drude-Lorentz (DL) model [2] which holds all over the spectrum (i.e., from visible to near infrared wavelengths).

Surface plasmon polaritons (SPPs) are typical electromagnetic (EM) waves that propagate along a metal-dielectric interface and whose amplitudes decay exponentially away from the interface. Because of their tighter spatial confinement and higher local field intensity, as well as high sensitivity to the permittivity function, SPPs have been used in various applications including sensing [3, 4], imaging [5], nano-photon detectors [6], enhanced second harmonic generation [7], surface enhanced Raman scattering [8], and many more. Such SPPs propagate not only at the interface of an isotropic metal and

an isotropic dielectric [9], but also at the interface between an isotropic metal and an anisotropic dielectric [10, 11]. Examples include the Dyakonov surface waves (DSWs) [12, 13] and Dyakonov surface plasmons (DSPs) [14] which have properties of both the Dyakonov surface waves and the SPPs. The DSWs have some unique characteristics, e.g., they are weakly localized and they propagate at the interface of two media at least one of which is anisotropic and the real parts of the permittivity functions are of opposite sign. Also, they are hybridized due to polarization of both the transverse electric (TE) and the transverse magnetic (TM) fields, and they are highly directional, i.e., they can exist only under certain conditions and in specific regimes [15].

Extensive and potential applications of SPPs and DSPs demand proper theoretical investigations together with convenient and controllable tools and techniques for coupling of EM waves and surface plasmons. Also, it has become possible to control the permittivity function of materials, and thereby enabling new approaches for the excitation of SPPs and DSPs due to the availability of non-conventional plasmonic materials such as transparent conductive materials and highly doped semiconductors [16, 17]. Efficient excitation of such surface waves have become possible with specially designed structures, e.g., metallic gratings [18–20], nanoslits [21] and uniaxial crystals [10, 11].

The necessary conditions together with the parameter regimes for the existence of DSPs and their dispersion properties at the interface of a metal and a uniaxial crystal has been studied by Li *et al.* [10] with the simple Drude model for  $\epsilon_p$  (without any absorption or damping constant). In another work, Moradi *et al.* [11] studied the similar theory of DSPs with the Drude model but in a doped InSb plasma and a uniaxial rutile (TiO<sub>2</sub>) crystal at THz frequencies [11]. However, the theory of DSPs at optical frequencies, especially in the short-wavelength spectra has not been advanced with the DL model to

\* apmisra@visva-bharati.ac.in; apmisra@gmail.com

† mshmansouri@gmail.com

‡ nkoddam2002@gmail.com

account for the contribution of both the intraband and higher-order interband transitions of electrons in metals.

In this work, our aim is to consider the DL model for the complex material permittivity, which holds for a wide range of wavelength spectra, and study the dispersion properties of DSPs at the interface of an isotropic gold metal and an anisotropic uniaxial crystal  $\text{TiO}_2$ . We show that the DL model is much more pronounced than the Drude model in the regimes of short-wavelength spectra ( $\lesssim 500$  nm), and the dispersion properties of DSPs are significantly modified.

## II. THEORETICAL FORMULATION

We consider a planar interface ( $x = 0$ ) of two media consisting of a semi-infinite isotropic metal with permittivity  $\epsilon_p$  occupying the space ( $x > 0$ ) and a semi-infinite anisotropic uniaxial optical crystal ( $x < 0$ ) with the permittivity tensor  $\epsilon_c$  and the optical axis  $OA$  of the crystal lying in the interface plane, i.e., the  $yz$ -plane. The principal diagonal elements of  $\epsilon_c$  are  $\epsilon_o$ ,  $\epsilon_o$  and  $\epsilon_e$  which represent the dielectric constants of the ordinary and extraordinary modes in the crystal [10–12]. We also assume that the propagation vector  $\mathbf{k}_p$  of DSPs is along the  $z$ -axis, making an angle  $\phi$  with  $OA$ . A schematic diagram of the system configuration is shown in Fig. 1. The traditional SPPs, which involve both the plasma motion and EM waves, are known to be excited by the pure TM mode. However, the DSPs, as in Fig. 1, may not be excited either by the pure TE or the pure TM wave fields, but by both the fields. In contrast to two evanescent fields of usual SPPs, the DSPs, which has a polarization hybridized nature, can have four evanescent wave fields: two TE and TM-like modes with an identical wave vector  $\mathbf{k}_p = (-ik_p, 0, q)$  and two ordinary-light (OL) and extraordinary-light (EL)-like modes with wave vectors  $\mathbf{k}_o = (-ik_o, 0, q)$  and  $\mathbf{k}_e = (-ik_e, 0, q)$ . Here,  $k_p$ ,  $k_o$  and  $k_e$  are determined by the following dispersion laws [10–12].

$$k_p^2 = q^2 - \epsilon_p, \quad (1)$$

$$k_o^2 = q^2 - \epsilon_o, \quad (2)$$

$$(q^2 \sin^2 \phi - k_e^2)/\epsilon_e + (q^2 \cos^2 \phi)/\epsilon_o = 1. \quad (3)$$

The permittivity function of the metal can be described by the Drude-Lorentz model as [2]

$$\epsilon_p(\omega) = \epsilon_\infty - \frac{\Omega_p^2}{\omega(\omega + i\gamma_d)} + \sum_{j=1}^m \frac{f_j \omega_p^2}{\omega_j^2 - \omega(\omega + i\gamma_j)}. \quad (4)$$

The combination of the first and the second terms on the right-hand side of Eq. (4) is referred to as the *intraband* part (i.e., the Drude model with free-electron effects) and the third term as the *interband* part (i.e.,

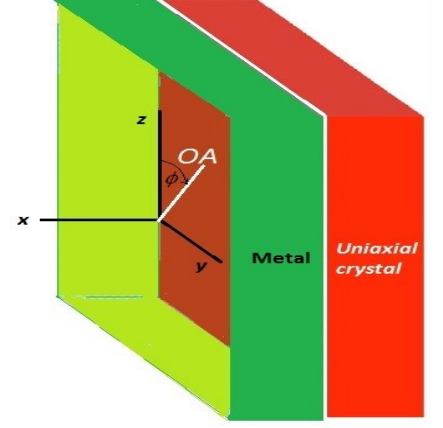


FIG. 1. A schematic diagram of a planar interface ( $x = 0$ ) between an isotropic metal ( $x > 0$ ) and an anisotropic uniaxial crystal ( $x < 0$ ) is shown. Here,  $OA$  is the optical axis making an angle  $\phi$  with the direction of propagation, i.e., the  $z$ -axis.

the Lorentz model with the effects of bound electrons). Also,  $\epsilon_\infty$  stands for the relative permittivity of the metal at high (infinite) frequency,  $\omega_p$  is the plasma oscillation frequency of the bulk metal,  $\Omega_p = \sqrt{f_0} \omega_p$  is the plasma frequency associated with the intraband transitions with oscillator strength  $f_0$  and  $\gamma_d$  is the damping constant. Furthermore,  $m$  is the number of high-energy oscillators with the resonant frequency  $\omega_j$ , weighting coefficient  $f_j$  and lifetime  $1/\gamma_j$  for  $j = 1, 2, \dots, m$ . The physical interpretations of the real and imaginary parts of the dielectric function are that while the real part determines the degree of polarization when the material is subjected to an electric field or magnetic field, the imaginary part determines that of absorption inside the medium.

As stated before, the Drude model is the simplest description of the permittivity function of metals and semi-conductors, and it holds for the intraband transition of free or conduction electrons. To account the net contribution of positive ion core, the parameter  $\epsilon_\infty$  may be introduced in the Drude model [1]. Though, the Drude model has been used in many physical situations to fit with experimental results (especially in the regimes of longer infrared wavelengths, i.e.,  $\lambda > 500$  nm [22]), it has some limitations, e.g., it diverges as  $\omega \rightarrow 0$ , it does not include the wave vector and it may not be valid for a short-wavelength spectra ( $\lesssim 500$  nm) where the contribution of interband transitions become important. However, in the present work, the very low-frequency limit, i.e.,  $\omega \rightarrow 0$  is not relevant as  $\omega \lesssim \omega_p$ . However, the divergence issue, if any, may be resolved by replacing the Drude model by the Linhard model [1].

In order that the DSPs exist at the interface of two media, the real parts of the wave vector components  $k_p$ ,

$k_o$ ,  $k_e$  and  $q$  must be positive. As in Refs. [10–12], the propagation angle is considered to be in the regime  $0 \leq \phi \leq \pi/2$ . Applying the appropriate boundary conditions, one can obtain the following dispersion relation for DSPs [10–12].

$$(k_p + k_e)(k_p + k_o)(\epsilon_p k_o + \epsilon_o k_e) = (\epsilon_e - \epsilon_p)(\epsilon_p - \epsilon_o)k_o. \quad (5)$$

We note that the permittivity function in Eq. (4) is complex with its real part may be positive or negative depending on the values of  $\epsilon_\infty$  and other parameters. However, we consider the case in which  $\omega \lesssim \omega_p$  (where the optical properties of a medium exhibit metal-like behaviors) and  $\Re \epsilon_p < 0$ ,  $\Re \epsilon_o$ ,  $\Re \epsilon_e > 0$  as in Refs. [10–12]. The conditions for the existence of DSPs in absence of any collision and using the Drude model has been discussed in detail in Ref. [10]. We, however, consider the collisional and resonance effects, and analyze the dispersion relation (5) numerically in the next section III.

### III. RESULTS AND DISCUSSION

In this section, we study the dispersion properties of Dyakonov surface plasmon oscillations that can propagate at the interface of an isotropic gold metal (Au) and a uniaxial crystal (TiO<sub>2</sub>) using the DL model for the permittivity of metals. To this end, we numerically solve Eq. (5) together with Eqs. (1) to (3), and consider the parameters that are relevant for gold metal [2] and uniaxial rutile [23]. All the frequencies including the surface wave frequency and the collisional frequency are normalized by the plasma frequency  $\omega_p$ , whereas the wave vector components are normalized by  $\omega_p/c$ , where  $c$  is the speed of light in vacuum. Since  $\epsilon_p$  is complex due to the damping constant  $\gamma_d$ , the other permittivity constants  $\epsilon_o$  and  $\epsilon_e$ , as well as the wave vector components  $k_p$ ,  $k_o$ ,  $k_e$  and  $q$  are also complex quantities. For the gold metal at room temperature, we consider the plasma density as  $n = 6 \times 10^{28} \text{ m}^{-3}$  such that  $\omega_p = 13.8 \times 10^{15} \text{ s}^{-1}$ . Also, we choose  $\epsilon_\infty = 1.2$ ,  $f_0 = 0.760$  and  $\gamma_d = 0.0058$  and the other parameter values as given in Table I and/or in Ref. [2]. The parameters for TiO<sub>2</sub> are considered as [23]  $\epsilon_o = (2.89)^2 + i(0.02)^2$  and  $\epsilon_e = (3.3)^2 + i(0.03)^2$  at the frequency  $\omega = 0.36$  (in terms of units,  $\omega \sim 5 \times 10^{15} \text{ s}^{-1}$  or  $\lambda \equiv 2\pi c/\omega \approx 400 \text{ nm}$ ). Due to limited source of experimental data for the DL model, we consider the effects of at most five interband transitions ( $m = 5$ ) in the gold metal.

Figure 2 displays the characteristics of the real parts of the wave vector components  $k_p$ ,  $k_o$ ,  $k_e$  and  $q$  against the propagation angle  $\phi$  corresponding to the Drude model (solid lines) and the DL model (dashed, dotted and dash-dotted lines) for the permittivity  $\epsilon_p$ . The effects of the intraband transitions of free electrons (solid lines) and the combined effects of both the intraband and multiple interband transitions of electrons (dashed, dotted and dash-dotted lines) are shown. In the short-wavelength spectra (below 500 nm), we choose  $\omega = 0.36$  ( $\lambda \sim 400$

nm) at which the values of the real parts of  $\epsilon_p$  for the Drude model and the DL model with  $m = 1, \dots, 5$  are negative. We find that the Drude model and the DL model with one interband transition predict almost the same behaviors. However, significant changes occur when more than three interband transitions are taken into account (see the dotted and dash-dotted lines). In all the cases, the wave number  $k_e$  decays, but  $k_p$ ,  $k_o$  and  $q$  increase with increasing values of  $\phi$  within the interval  $0 \leq \phi \leq \pi/2$ . It is interesting to note that while the magnitudes of the wave number  $q$  increase with the effects of different multiple interband transitions [see subplot (d)], those of  $k_p$ ,  $k_o$  and  $k_e$  may increase or decrease [see subplots (a) to (c)] depending on the values of  $m = 3, 4$  or  $5$ . It means that the DSPs are sensitive to the change of permittivity either of the isotropic metal or of the anisotropic crystal, and that because of the decreasing natures of  $k_e$  in the rutile substrate and increasing natures of  $k_p$  or  $q$  in the metal, the DSPs may be said to be moderately localized [15]. Note here that these qualitative features, as shown in Fig. 2, remain almost the same in a wide range of wavelength spectra 200 to 650 nm or the frequency range  $3.8$  to  $9.4 \times 10^{15} \text{ s}^{-1}$ .

One important characteristic of DSPs is the penetration depth or skin depth, i.e.,  $k_p^{-1}$  in the metallic gold and  $k_e^{-1}$  in the rutile substrate. Since the penetration depth determines the coupling strength between the surface plasmons and other elements of photonic materials, its enhancement is most desirable. From the subplots (a) and (b) of Fig. 3, it is clear that the penetration depths in the metal and uniaxial crystal increase with increasing values of  $\phi$  except those at  $m = 5$  in which they decrease with increasing values of  $\phi$ . Such an enhancement of the penetration depth for  $m = 1$  to  $4$  reaches maximum for perpendicular orientation ( $\phi = \pi/2$ ) and minimum for parallel orientation ( $\phi = 0$ ) of the optical axis  $OA$ . So, it follows that the perpendicular orientation is more preferable for transmission of signals in the optical wavelength. Furthermore, the penetration depth is higher at  $m = 3$  and  $m = 5$  interband transitions compared to that at  $m = 4$  and no interband transition. The enhancement is significant at  $m = 5$  (see the dash-dotted lines, scaled as  $k_p^{-1}/2$  and  $k_e^{-1}/4$ ) though at this transition the penetration depth decreases with  $\phi$  which may favor better confinement of DSPs to the interface [15]. Thus, in contrast to four interband transitions, when five or higher interband transitions come into play in metals the parallel orientation is more desirable than the perpendicular orientation for transmission of signals.

The dispersion curves, i.e., the plots of the wave frequency (real part) against the wave number  $q$  of DSPs are shown in Fig. 4 in two different cases: (a) the effect of multiple interband transitions and (b) the effect of the angle of propagation or the orientation of the optical axis. From the subplot (a), it is found that when no interband transition is considered (the solid line), the behavior of the dispersion curve remains the same as in Refs. [10, 11], i.e., the wave frequency approaches a con-

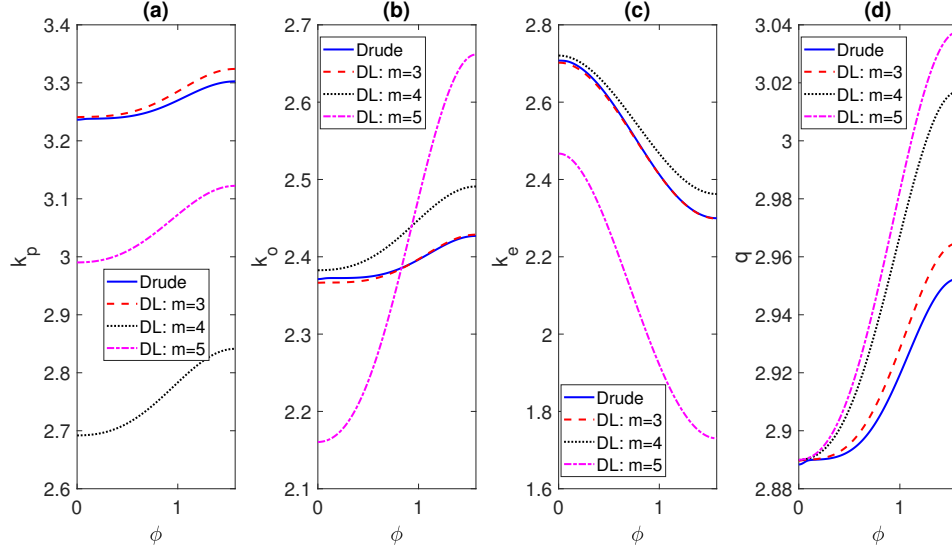


FIG. 2. The real parts of the wave numbers (a)  $k_p$ , (b)  $k_o$ , (c)  $k_e$  and (d)  $q$  are plotted against the propagation angle  $\phi$  to show the effects of multiple interband transitions for a particular value of the wave frequency  $\omega = 0.36$  at which  $\epsilon_0 = (0.89)^2 + i(0.02)^2$  and  $\epsilon_e = (0.36)^2 + i(0.03)^2$  relevant for  $\text{TiO}_2$  uniaxial crystals [23]. Also,  $\epsilon_\infty = 1.2$  and other parameter values relevant for gold metals are given in Table I. The dash-dotted lines in subplots (b) and (c) are scaled as  $2k_o$  and  $2k_e$  respectively.

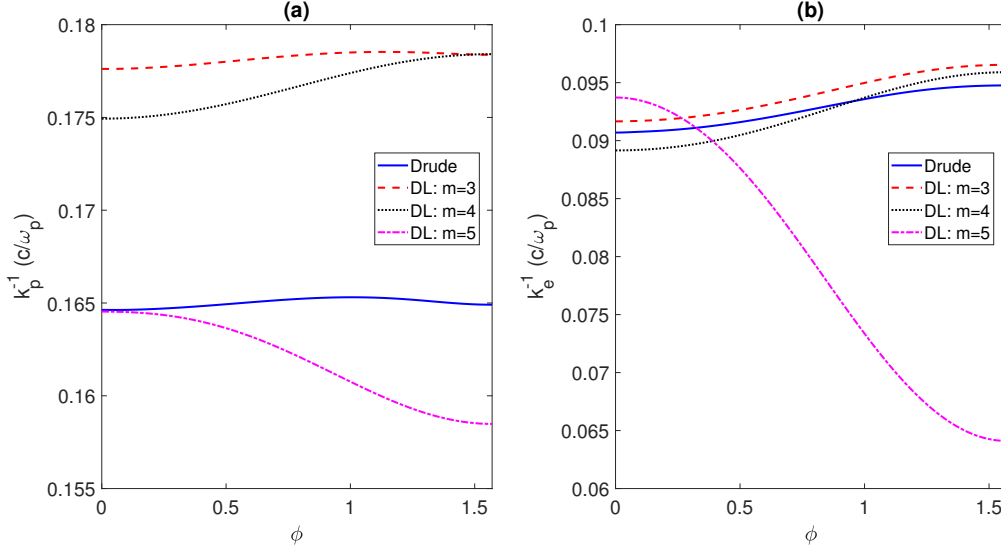


FIG. 3. The penetration depths of DSPs are shown (a) in the isotropic metal (b) in the uniaxial crystal for different interband transition effects to the material permittivity. The dash-dotted lines are scaled as  $k_p^{-1}/2$  and  $k_e^{-1}/4$

stant value after it starts increasing within a short-range of values of  $q$ . However, when multiple interband transitions are considered together with the intraband transition, the DL model gives a significant modification of the dispersion curves, especially for ( $m > 3$ ). In contrast to the Drude model and previous investigations [10, 11], the DSPs clearly display dispersion as well as resonant behaviors within a short-range of values of  $q$  (see the dotted and dash-dotted lines). Physically, these occur due to the contribution from interband transitions of bound

electrons in the metal gold to the permittivity function  $\epsilon_p$  with different oscillation frequencies  $\omega_j$  of the resonant modes. From the subplot (a), it is also clear that the Drude model is no longer applicable when the effects of more than three interband transitions come into the picture in the short-wavelength spectra:  $\lambda \lesssim 500$  nm. Furthermore, the wave frequency decreases with the effects of multiple interband transitions ( $m > 2$ ) in the DL model except in the regime of small  $q$ , i.e.,  $q \lesssim 1$ .

The direction of propagation  $\phi$  with the optical axis

also plays an important role in the characteristics of DSPs as depicted in Fig. 4 (b). It is seen that the wave frequency in both the cases (with the Drude and the DL models) is significantly reduced with a reduction of the angle of propagation (see the solid and dashed lines for the Drude model, and dotted and dash-dotted lines for the DL model). So, by reducing or increasing the angle of propagation from an initial value one can have a wide range of wavelength spectra for DSPs including the regime with  $\lambda \lesssim 500$  nm. In this way, the wave frequency of DSPs can be tuned with changing the orientation of the optical axis.

TABLE I. The parameter values relevant for the gold metal (Au) as in Ref. [2] for the Drude-Lorentz model with  $\gamma_d = 0.053$  eV [ $0.0805 \times 10^{15} \text{ s}^{-1}$ ] and  $\omega_p = 9.1$  eV [ $13.8 \times 10^{15} \text{ s}^{-1}$ ] for which  $n = 6 \times 10^{28} \text{ m}^{-3}$ .

| $f_j$ | $\gamma_j$<br>(eV) | $\gamma_j$<br>( $10^{15} \text{ s}^{-1}$ ) | $\omega_j$<br>(eV) | $\omega_j$<br>( $10^{15} \text{ s}^{-1}$ ) |
|-------|--------------------|--|--------------------|--|
| 0.024 | 0.241              | 0.3661                                     | 0.415              | 0.6304                                     |
| 0.010 | 0.345              | 0.5241                                     | 0.830              | 1.2609                                     |
| 0.071 | 0.870              | 1.3216                                     | 2.969              | 4.5102                                     |
| 0.601 | 2.494              | 3.7886                                     | 4.304              | 6.5382                                     |
| 4.384 | 2.214              | 3.3633                                     | 13.32              | 20.2344                                    |

We have mentioned that the DSPs are hybridized due to polarization of both the TE and TM modes. In order to distinguish the polarization characteristics, we define two factors  $P_{E/M}$  and  $P_{o/e}$ , respectively, as the amplitude ratios between the TE and TM modes in the isotropic metal and between the ordinary and extraordinary modes in the uniaxial crystal as [11]

$$P_{E/M} = \frac{q^2 - k_e k_o - \epsilon_o}{i\epsilon_o(k_e + k_p) \tan \phi + ik_e(\epsilon_o - q^2 - k_o k_p) \cot \phi}, \quad (6)$$

$$P_{o/e} = \frac{i(k_p + k_e) \tan \phi}{\epsilon_o - q^2 - k_o k_p}. \quad (7)$$

The absolute values of  $P_{E/M}$  and  $P_{o/e}$  are plotted against  $\phi$  as shown in Fig. 5. It is found that for these ratios, the Drude model and the DL model with three interband transitions ( $m = 3$ ) predict almost the same results, however, it is significantly modified with  $m > 3$  [see the dashed lines in subplots (a) and (b)]. The values of both the ratios  $|P_{E/M}|$  and  $|P_{o/e}|$  increase with the effects of higher-order interband transitions of electrons. However, the ratio  $|P_{E/M}|$  reaches its maximum at an intermediate value of  $\phi$  and then decreases to have a cut-off at  $\phi = \pi/2$ . Such cut-offs may be different for different values of either  $\epsilon_p$  or both  $\epsilon_o$  and  $\epsilon_e$ . Although, the DSPs have been known to be TM-dominant [11], such an increase of  $|P_{E/M}|$  in the present analysis indicates that the contribution of the TE-polarization may no longer be negligible, especially at higher-order interband transitions of electrons. On the other hand, the effect of the

interband transitions on the ratio  $|P_{o/e}|$  in the uniaxial crystal is also found to be significant and that its values become higher and higher with increasing values of  $\phi$ .

#### IV. CONCLUSION

We have studied the dispersion properties of Dyakonov surface plasmons (DSPs) propagating along the interface of an isotropic metallic plasma [gold (Au)] and an anisotropic uniaxial crystal [Rutile (TiO<sub>2</sub>)] using the Drude-Lorentz (DL) model for the dielectric permittivity  $\epsilon_p$  of metals. The DL model is considered to take into account the effects of both the *intraband* transition of free electrons and *interband* transitions of bound electrons in metals. The higher-order interband transitions of bound electrons are very common especially in practical metals and these occur due to the excitation by the high-energy photons. In the short-wavelength spectra ( $\lambda \lesssim 500$  nm), since the interband transitions occur in the gold metal, the DL model is more appropriate than the Drude model for the description of  $\epsilon_p$ . It is found that the contributions of multiple interband transitions, as well as, the orientation ( $\phi$ ) of the optical axis significantly modify the wave vector components  $k_p$  and  $q$  of the TE/TM modes in the isotropic metal and  $k_o$  and  $k_e$  of the ordinary and extraordinary modes in the anisotropic crystal. The modifications are noticeable when the contribution of three or more interband transitions come into the picture. The values of the wave numbers decrease or increase depending on the values of  $\phi$  and the order of interband transitions  $m$  in the permittivity  $\epsilon_p$ . We have also shown that the penetration depths of DSPs in the metal and uniaxial crystal increase with increasing values of  $\phi$  in the whole interval  $0 \leq \phi \leq \pi/2$  and when the effects of multiple interband transitions ( $m < 5$ ) are considered. However, the exception occurs at  $m = 5$  in which case the penetration depth decreases with increasing values of  $\phi$ . The enhancement of the penetration depth becomes significantly higher at  $m = 3$  and  $m = 5$  compared to those at  $m = 1$  to 4 and with no interband transition. So, an appropriate choice of the orientation of the optical axis and the multiple interband transitions of electrons may be required for the (i) better confinement of DSPs to the interface having lower penetration depth and (ii) transmission of optical signals with higher penetration depth of DSPs.

A numerical solution of the dispersion equation also reveals that in contrast to the Drude model or DL model with up to three interband transitions, the real part of the wave frequency of DSPs exhibits strong dispersion and resonance with multiple peaks at higher-order ( $m > 3$ ) interband transitions. We have also calculated the absolute amplitude ratios between the TE and TM modes in the isotropic metal ( $|P_{E/M}|$ ), as well as between the ordinary and extraordinary modes in the uniaxial crystal ( $|P_{o/e}|$ ). It is shown that in contrast to the previous investigation [11] with the Drude model in semiconduc-

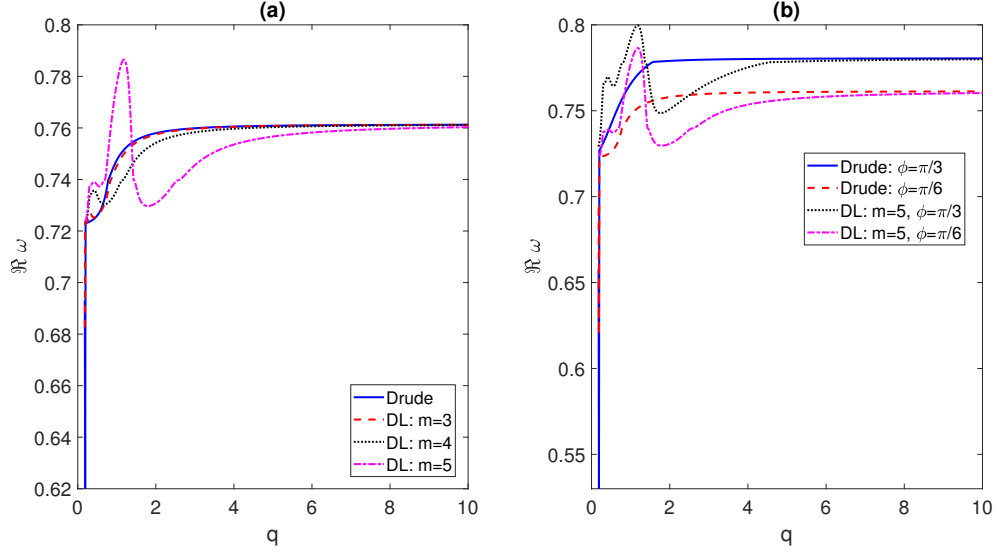


FIG. 4. Plots of the real part of the wave frequency against the wave number  $\Re q$  of DSPs to show the effects of (a) the multiple interband transitions for a fixed  $\phi = \pi/6$  and (b) the angle of propagation. We choose  $\epsilon_0 = (2.89)^2 + i(0.02)^2$  and  $\epsilon_e = (3.3)^2 + i(0.03)^2$  relevant for  $\text{TiO}_2$  uniaxial crystals at a frequency  $\sim 3 \times 10^{15} \text{ s}^{-1}$  [23]. Also, we consider  $\epsilon_\infty = 10.0$  and other parameter values relevant for gold metals as given in Table I.

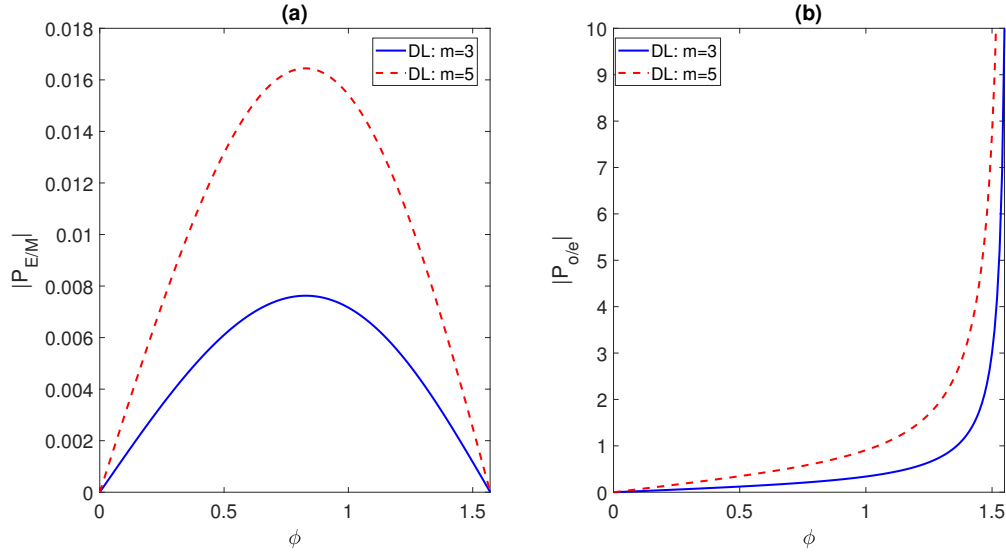


FIG. 5. The absolute values of the hybridization factors (a)  $P_{E/M}$  and (b)  $P_{o/e}$  are plotted against the propagation angle  $\phi$ . The effects of the interband transitions with  $m > 3$  are seen to be significant.

tor plasmas where the contribution of the TE-mode was reported to be negligible in the excitation of DSPs, the contribution of the TE mode to DSPs may not be negligible when more than three interband transitions are taken into account.

To conclude, the DSPs can be used as a sensor and switching system due to their high sensitivity to the relative values of the permittivities of the two media. Also, since the wave frequency can be tuned with changing the orientation of the optical axis, the DSPs may be a good

candidate for the transportation of directional EM signals. The theoretical results should be useful to design new experiments for the excitation of surface EM waves that can propagate along the interface of an isotropic gold metal and an anisotropic uniaxial crystal (rutile) at optical frequencies. Finally, it has been found in Ref. [24] that any change of thermodynamic temperature can have strong influence on the field enhancement and absorption characteristics of plasmonic devices. In the light of this research, the present work could be advanced with

a more general model by considering the temperature dependency of the plasma frequency  $\Omega_p$  and the damping coefficient  $\gamma_d$  in the Drude model, i.e., the Drude-Lorentz-Temperature (DLT) model for the material permittivity  $\epsilon_p$ . However, this study is left for future work.

## ACKNOWLEDGMENTS

This work was supported by Science and Engineering Research Board (SERB), Govt. of India with Sanction order no. CRG/2018/004475 dated 26 March 2019.

- 
- [1] A. V. Andrade-Neto, Revista Brasileira de Ensino de Fisica **39**, e2304 (2017) [doi: 10.1590/1806-9126-RBEF-2016-0206].
  - [2] D. Rakić, A. B. Djurišić, J. M. Elazar, and M. L. Majewski, Appl. Optics **37**, 5271 (1998).
  - [3] J. Homola, S. S. Yee, and G. Gauglitz, Sens. Actuat. B: Chem. **54**, 3 (1999).
  - [4] T. Chung, S-Y Lee, E. Y. Song, H. G. Chun, and B. Lee, Sensors **11**, 10907 (2011).
  - [5] X. Zhang and Z. W. Liu, Nat. Mater. **7**, 435 (2008).
  - [6] L. Tang, S. E. Kocabas, S. Latif, A. K. Okyay, D-S Ly-Gagnon *et al.*, Nat Photonics **2**, 226 (2008).
  - [7] C. K. Chen, A. R. B. de Castro, and Y. R. Shen, Phys. Rev. Lett. **46**, 145 (1981).
  - [8] H. Metiu, *Surface Enhanced Raman Scattering*, edited by R. K. Chang and T. E. Furtak (Plenum, New York, 1982).
  - [9] X. Wang, Y. Deng, Q. Li, Y. Huang, Z. Gong, K. B. Tom, and J. Yao, Light: Science & Applications **5**, e16179 (2016) [doi:10.1038/lsa.2016.179].
  - [10] R. Li, C. Cheng, F-F Ren, J. Chen, Y-X Fan, J. Ding, and H-T Wang, Appl. Phys. Lett. **92**, 141115 (2008).
  - [11] M. Moradi and A. R. Niknam, Phys. Rev. B **98**, 085403 (2018).
  - [12] M. I. D'yakonov, Soviet Phys. JETP **67**, 714 (1988).
  - [13] N. S. Averkiev and M. I. Dyakonov, Optics and Spectroscopy (USSR) **68**, 653 (1990).
  - [14] Z. Jacob and E. E. Narimanov, Appl. Phys. Lett. **93**, 221109 (2008).
  - [15] O. Takayama, A. Bogdanov, and A. V. Lavrinenko, J. Phys.: Condens. Matter **29**, 463001 (2017).
  - [16] J. Park, J-H Kang, X. G. Liu, M. L. Brongersma, Sci. Rep. **5**, 15754 (2015).
  - [17] P. R. West, S. Ishii, G. V. Naik, N. K. Emani, V. M. Shalaev *et al.* Laser Photon Rev. **4**, 795 (2010).
  - [18] R. H. Ritchie, E. T. Arakawa, J. J. Cowan, and R. N. Hamm, Phys. Rev. Lett. **21**, 1530 (1968).
  - [19] O. Takayama *et al.*, Semiconductors **52**, 442 (2018).
  - [20] W. Ma *et al.*, Nature **562**, 557 (2018).
  - [21] H. F. Shi, C. T. Wang, C. L. Du, X. G. Luo, X. C. Dong *et al.*, Opt. Express **13**, 6815 (2005).
  - [22] Y. Li, *Plasmonic Optics: Theory and Applications*, Chap. 1 (SPIE Digital Library, 2017)[doi: 10.1117/3.2263757].
  - [23] J. R. Devore, J. Opt. Soc. Am. **41**, 416 (1951).
  - [24] A. Alabastri, S. Tuccio, A. Giugni, A. Toma, C. Liberale, G. Das, F. De Angelis, E. Di Fabrizio, and R. P. Zaccaria, Materials **6**, 4879 (2013).